

Slope stability analysis based on SBFEM and multistage polytree-based refinement algorithms

Xiupeng Nie^{a,b}, Kai Chen^{a,b,*}, Degao Zou^{a,b}, Xianjing Kong^{a,b}, Jingmao Liu^{a,b}, Yongqian Qu^{a,b}

^a The State Key Laboratory of Coastal and Offshore Engineering, Dalian University of Technology, Dalian, Liaoning 116024, China

^b School of Hydraulic Engineering, Dalian University of Technology, Dalian, Liaoning 116024, China

ARTICLE INFO

Keywords:

Slope stability analysis
Scaled boundary finite element method
Strength reduction method
Polytree-based mesh refinement algorithm
Refinement indicator

ABSTRACT

A fresh slope stability analysis method is proposed in this paper, with combining scaled boundary finite element method (SBFEM), strength reduction method (SRM) and polytree-based mesh refinement algorithm. Firstly, SBFEM and SRM (SBFEM-SRM) formulation are innovatively combined to conduct the slope stability analysis with a coarse analysis mesh. Secondly, a shear-strain-based refinement indicator is introduced to determine the elements that need to be refined, then multistage local mesh refinement can be implemented recursively on-demand via the independently developed polytree-based refinement algorithm. The accuracy and superiority of SBFEM-SRM are firstly verified using a simple slope example. The effectiveness and applicability of SBFEM-SRM combined with the polytree-based refinement algorithm is demonstrated by using two examples, including a multilayered nonhomogeneous soil slope and an actual test embankment. The advantages of different methods can be inherited in the presented method, wherein flexible polygonal elements can be solved directly, and making a strong adaptability for complex geometry equipped. Moreover, the computational burden would be alleviated efficiently without compromising accuracy, benefiting from local adaptive mesh refinement strategy. And inspired by this, the proposed method can be briefly extended to 3D slope stability analysis, wherein the application performance will be more significant.

1. Introduction

Slope is one of the most universal geotechnical structures serving for the economic and social development, and its application field involves many engineering practices, such as highway, dam, and open pit mine and so on. Therefore, as a pivotal infrastructure, the slope has increasingly attracted great attention of geotechnical researchers and has naturally become a popular research object in the geotechnical engineering field (e.g. Ke et al., 2019; Gao et al., 2020). With the continuous improvement of infrastructure technology and construction equipment, a growing number of slopes are put into production in more unpredictable circumstances and more complex working conditions. Under this circumstance, the stability of these slopes is closely related to the development of economy and society and the safety of people, so it becomes necessary and indispensable to carry out research on the stability assessment of such slopes.

For decades, much efforts have been made dedicating to the aim of predicting the slope stability extent and preventing the serious collapse consequence. These contributions can be categorized into three groups:

limit equilibrium (LE) method, limit analysis (LA) method and finite element (FE) method. LE is a most widely applied approach because of its simplicity (Krahn 2003; Tang et al., 2017; Metya et al., 2021), yet its solution is considered to unprecise due to the idealized mechanical assumptions with the purpose of weakening the difficulty in solving solution, the inability of LE in predicting the evolution track of the failure zone shape of slope also limits its further pervasive application to a great extent in slope stability. In addition, LA has also played a progressively crucial role in slope stability design, it is capable of providing concise calculation process and determining rigorous bounds on the limit state solutions (Xu et al., 2018; Li and Yang 2018), and thus gains a extend range of applications in slope stability (Ausilio et al., 2000; Michalowski and Drescher 2009; Pang et al., 2020). However, there exists difficulty in establishing the upper or lower bound theorem formulation in terms of dealing with complex slope configurations and irregular soil deposit problems, this disadvantage imposes specific obstacles to its widespread application. Alternatively, FE has been considered a powerful and comprehensive avenue to handle slope stability evaluation due to its advantage over LE and LA. On the one hand, FE can be used to calculate

* Corresponding author at: The State Key Laboratory of Coastal and Offshore Engineering, Dalian University of Technology, Dalian, Liaoning 116024, China.
E-mail address: chenkai@dlut.edu.cn (K. Chen).

expected slope deformations and the growth of plastic zone without prior assumptions once a realistic stress–strain constitutive model is assigned to the soil material (Khosravi and Khabbazi 2012; Kim and Lee 1997; Griffiths and Lane 1999). Moreover, FE is highly qualified to deal with complex slope geometry and loading sequence encountered frequently in geotechnical structure (Kim and Lee 1997), which are tricky issues in the LE and LA approaches. More recently, slope stability analyses through FE have been substantially exploited, Kontoe et al. (2013) conducted the pseudo-static finite element analysis to accurately and time-saving simulate the in situ, stresses prior to seismic loading, the sensitivity of the pseudo-static analysis results to finite element mesh was also explored, thus successfully providing reference theoretical guidance for practical engineering. Gao et al. (2018) investigated the influences of reservoir water level drawdown on slope stability through a series of numerical simulations so as to extend FE to different hydrological and meteorological conditions. Summersgill et al. (2018) performed two-dimensional plane-strain finite-element analyses to simulate the excavation of a slope in a stiff clay and the interaction of vertical piles within the slope. Therefore, FE seems to be a more reliable and adaptable handling technique in modeling and evaluating the performance of slope.

Generally, the classical slope stability analysis process mainly involves two simultaneous assignments: searching for the safety factor and tracking down the critical failure surface associated with the safety factor. However, FE is just a process analysis method but not a limit analysis method, it cannot give the specific definition and clear judgement criterion concerning the limit state of slope, and in this way yielding a reliable safety factor is difficult (Liu et al., 2015b). Alternatively, the strength reduction method (SRM), first introduced by Zienkiewicz et al., (1975), has been given extensive concern from majority researchers and achieved long-term progress in the aspect of slope stability analysis because of its feasibility and reliability in searching for the status on the verge of instability. Naturally, to realistically simulate the progressive instability process and finally determine the limit state of the slope, FE combined with strength reduction method (FE-SRM) become progressively prevailing over the past few decades, and large quantities of studies using FE-SRM approach have been dedicated to slope stability analysis. Sun et al. (2021) developed a nonlinear FE-SRM for analyzing the stability of uniform slopes with the general nonlinear failure criterion. Li et al. (2022) conducted FE-SRM to locate the critical slip surface and assessing the safety factor of crack slope. Kontoe et al. (2022) performed two-dimensional plane-strain hydro-mechanically coupled FE-SRM analyses to simulate the excavated slope by considering both strain-softening and non-softening response of materials, the research theoretically revealed the interaction between soil and pile with important implications for design practice. FE-SRM can only access a unique safety factor of slope and rather precisely locate the corresponding critical failure zone without specifying its shape and location in advance, thus FE-SRM is regarded as a powerful tool for slope stability analysis.

In two-dimensional(2D) problem, traditional FE is often discretized into simplex elements, viz., triangles/quadrilaterals. However, convergent rates of triangular elements in terms of many problems are unsatisfactory (Chi et al., 2014). Meanwhile, quadrilateral elements could be very awkward when dealing with highly complex structures (Chau et al., 2017). The polygonal element has been used as a substitution recently due to its flexibility in mesh generation and high quality in computational result and convergence degree. In fact, the accuracy of the solution obtained from the FE hinges largely on the mesh density. To improve the accuracy, one of the most efficient approaches is locally refine the mesh. The idea of multistage local mesh refinement is rarely applied to slope engineering, only Cramer et al., (1999) used quadtree concept to solve the ultimate bearing capacity problem of slope. However, the mesh decomposition would lead to the presence of hanging nodes along the edge of elements, the constraint treatment technique for hanging nodes using FE by Cramer et al., (1999) usually requires a

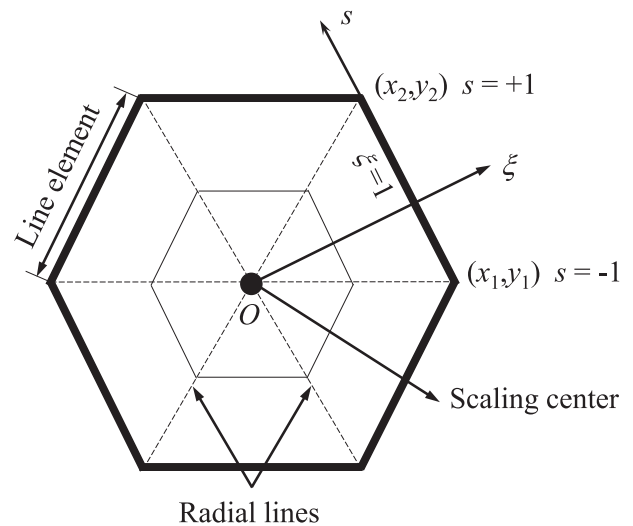


Fig. 1. Schematic diagram of the scaled boundary polygon.

complex algorithm (Zander, 2016) and is difficult to be implemented in three-dimensional problem and meshes with unsymmetric and/or multi-level hanging nodes (Byfut, 2017). Recently, a flexible polytree-based mesh refinement algorithm has been preliminarily implemented which can achieve a local mesh refinement function through the idea of polytree decomposition. By means of a refinement indicator, the polytree mesh refinement algorithm can automatically identify the location of elements that need to be refined. In recent years, thanks to its powerful capability in local mesh refinement, the application of polygonal finite elements into polytree mesh refinement algorithm has become increasingly popular (Chau et al., 2017; Nguyen et al., 2016; Nguyen et al., 2019). In terms of handling hanging node problem, special techniques have been applied to developed, among which the scaled boundary element method (SBFEM) has gained much attention from researchers in the recent years (Ooi et al., 2012; Ooi et al., 2017; Pramoda et al., 2018).

SBFEM is a numerical method first developed by Wolf and Schanz (2004), it only requires the discrete process towards the boundary of elements so it has the advantage of dimension reduction; Moreover, the applied semi-analytical approach eliminates less accurate solutions caused by the singularity of shape function derivatives near elements. These advantages have made SBFEM widely recognized by researchers and applied in various fields, such as the electrostatic problem (Liu and Lin 2012), dam simulations (Chen et al., 2017a; Chen et al., 2018a; Zou et al., 2017), Cosserat continuum analysis (Chen et al., 2021), and crack propagation (Ooi et al., 2013; Jiang et al., 2019; Qu et al., 2020). These applications strongly prove SBFEM to be an effective coping mean in solving practical problems.

In this paper, we conduct a fresh slope stability analysis, with combining SBFEM, SRM and flexible polytree-based mesh refinement algorithm, both the safety factor and the generalized shear strain (GSS) are used as the evaluation indexes of slope stability. The slope fillings are modelled as perfect elasto-plastic materials following the Mohr-Coulomb failure criterion. Based on a shear-strain-based refinement indicator, multistage local mesh refinement can be achieved via an independently developed polytree-based mesh refinement algorithm. The effectiveness and accuracy of the proposed method is then verified by using several examples, it is evident that the proposed method has very good accuracy and adaptability in slope stability evaluation, it could not only enhance the calculation precision but reduce the calculation cost. Moreover, as a multistage mesh refinement process is performed, the analysis would tend to be a more desired solution.

The rest of the paper is organized as follows: Overview of SBFEM is described in Section 2. The flexible polytree-based mesh refinement algorithm and the realization process of local mesh refinement are

described in Section 3. Section 4 gives introduction of SRM theory. Slope failure criterion and mesh refinement basis is provided in Section 5. Numerical example verifications are presented in Section 6. Finally, the concluding remarks are presented in Section 7.

2. Overview of SBFEM for perfect elasto-plastic materials

The SBFEM is a semi-analytical method which was first introduced by Wolf and Schanz (2004). In 2D problem, unlike the traditional FE method which limits the element discretization type to the simplex shapes such as triangles and quadrilaterals, the SBFEM allows discretization of arbitrary sided polygons. Fig. 1 shows a schematic of a typical polygon modelled by the SBFEM, and the scaling center O in the geometric center of the polygon is introduced, any point on the polygon boundary must be visible to the scaling center. Within SBFEM, each boundary of the polygonal elements is discretized with one-dimensional line elements in a local coordinate η that varies from -1 to 1 . Inside the polygon, a radial coordinate ξ is established from 0 at the scaling center to 1 at the polygon boundary (see Fig. 1). The coordinates (x, y) of any point in Cartesian coordinates can be converted to scaling coordinates (ξ, s) as follows.

$$x(\xi, s) = x_0 + N(s)x_b \quad (2-1a)$$

$$y(\xi, s) = y_0 + N(s)y_b \quad (2-1b)$$

$$N(s) = \begin{bmatrix} N_1 & 0 & N_2 & 0 & \dots & N_m & 0 \\ 0 & N_1 & 0 & N_2 & \dots & 0 & N_m \end{bmatrix} \quad (2-2)$$

where x_0, y_0 are scaling center coordinates, x_b, y_b are the nodal coordinates vector of the line element on the boundary, and $N(s)$ is the shape function matrix of the line element contains m nodes.

In the SBFEM, the approximation displacement at any point in the scaling coordinates of a subdomain can be written as.

$$u(\xi, s) = N(s)u(\xi) \quad (2-3)$$

where $u(\xi)$ is the nodal displacement functions along the radial line connecting the scaling center and the node on the boundary. The partial differential equations of equilibrium of a polygon can be formulated by virtual work principle (Ooi et al., 2012) or weighted residual method (Chen et al., 2017b). Both equilibrium equations can solve the radial displacement functions $u(\xi)$ as follows.

$$E_0 \xi^2 u(\xi),_{\xi\xi} + (E_0 + E_1 + E_1)\xi u(\xi),_{\xi} - E_2 u(\xi) + F(\xi) = 0 \quad (2-4)$$

where the coefficient matrices E_i ($i = 0, 1, 2$) is related only to the geometry and material properties of the subdomain, which has been given in Eq. (2.6). $F(\xi)$ is a load vector that includes only the body load. Then, the equation can be rewritten as:

$$E_0 \xi^2 u(\xi),_{\xi\xi} + (E_0 - E_1 + E_1)\xi u(\xi),_{\xi} + (E_1 - E_2)u(\xi) + \omega^2 M_0 \xi^2 u(\xi) = 0 \quad (2-5)$$

with the following equations:

$$E_0 = \int_{-1}^{+1} B_1 D B_1 |J| ds \quad (2-6a)$$

$$E_1 = \int_{-1}^{+1} B_2 D B_1 |J| ds \quad (2-6b)$$

$$E_2 = \int_{-1}^{+1} B_2 D B_2 |J| ds \quad (2-6c)$$

$$M_0 = \int_{-1}^{+1} \rho N(s)^T N(s) |J| ds \quad (2-6d)$$

where B_1 and B_2 are strain-displacement transition matrices, D is a constitutive matrix, ρ is the material density, and J is the Jacobian matrix of the coordinate transformation. Eq. (2.5) is a linear second-order matrix-form differential equation, by using the process for calculating the eigenproblems in Eq. (2.5), which has been presented in (Ooi et al., 2012; Chen et al., 2017b), the radial displacement functions $u(\xi)$ can be derived as.

$$u(\xi) = \psi_u \xi^{-S_n} \psi_u u_b \quad (2-7)$$

where S_n are the subset of the real parts of the eigenvalues, which include two zeros and negative numbers, and ψ_u are the eigenvectors corresponding to S_n , depending on the DOFs of a polygonal finite element. u_b is the nodal displacement vector on the element boundary ($\xi = 1$). Substituting Eq. (2.7) into Eq. (2.3), the displacement field $u(\xi, s)$ can be expressed by.

$$u(\xi, s) = N(s) \psi_u \xi^{-S_n} \psi_u u_b \quad (2-8)$$

Therefore, the polygon element displacement shape functions $\Phi(\xi, s)$ can be extracted from the right side of Eq. (2.8), which are given in the following form.

$$\Phi(\xi, s) = N(s) \psi_u \xi^{-S_n} \psi_u \quad (2-9)$$

In SBFEM, the strain field $\epsilon(\xi, s)$ in the scaling coordinates was proposed by Wolf and Schanz (2004) as.

$$\epsilon(\xi, s) = B_1(s)u(\xi),_{\xi} + \frac{1}{\xi} B_2(s)u(\xi) \quad (2-10)$$

Substituting the radial displacement functions $u(\xi)$ into Eq. (2.10), the strain field can be modified in the form of u_b as.

$$\epsilon(\xi, s) = (B_1(s) \psi_u S_n + B_2(s) \psi_u) \xi^{-S_n} \psi_u u_b \quad (2-11)$$

where $B_1(s)$ and $B_2(s)$ are transformation coefficient matrices that are expressed as:

$$B_1(s) = \frac{1}{|J|} \begin{bmatrix} y(s),_s & 0 \\ 0 & -x(s),_s \\ -x(s),_s & y(s),_s \end{bmatrix} N(s) \quad (2-12a)$$

$$B_2(s) = \frac{1}{|J|} \begin{bmatrix} -y(s) & 0 \\ 0 & x(s) \\ x(s) & -y(s) \end{bmatrix} N(s),_s \quad (2-12b)$$

Using Hooke's law, the corresponding stress field σ can also be expressed as.

$$\sigma(\xi, s) = D \epsilon(\xi, s) \quad (2-13)$$

where D is the elastic constitutive matrix. Substituting $\epsilon(\xi, s)$ in Eq. (2.11) into Eq. (2.13), the stress field $\sigma(\xi, s)$ can be naturally obtained.

In perfect elasto-plastic analysis, the incremental strain field consists of the incremental elastic strain increment and the plastic strain increment, as in Eq. (2.14). Using the associated flow rule, the plastic strain increment can be expressed by the yield functions F and the plastic multiplier $\Delta\lambda$, which is formulated in Eq. (2.15) as.

$$\Delta\epsilon = \Delta\epsilon_e + \Delta\epsilon_p \quad (2-14)$$

$$\Delta\epsilon_p = \frac{\partial F}{\partial \sigma} \Delta\lambda \quad (2-15)$$

Substituting Eq. (2.15) into Eq. (2.13), the stress field increment $\Delta\sigma$ can be expressed as.

$$\Delta\sigma = D_{ep} \Delta\epsilon \quad (2-16)$$

where D_{ep} is the perfect elasto-plastic constitutive matrix, and the

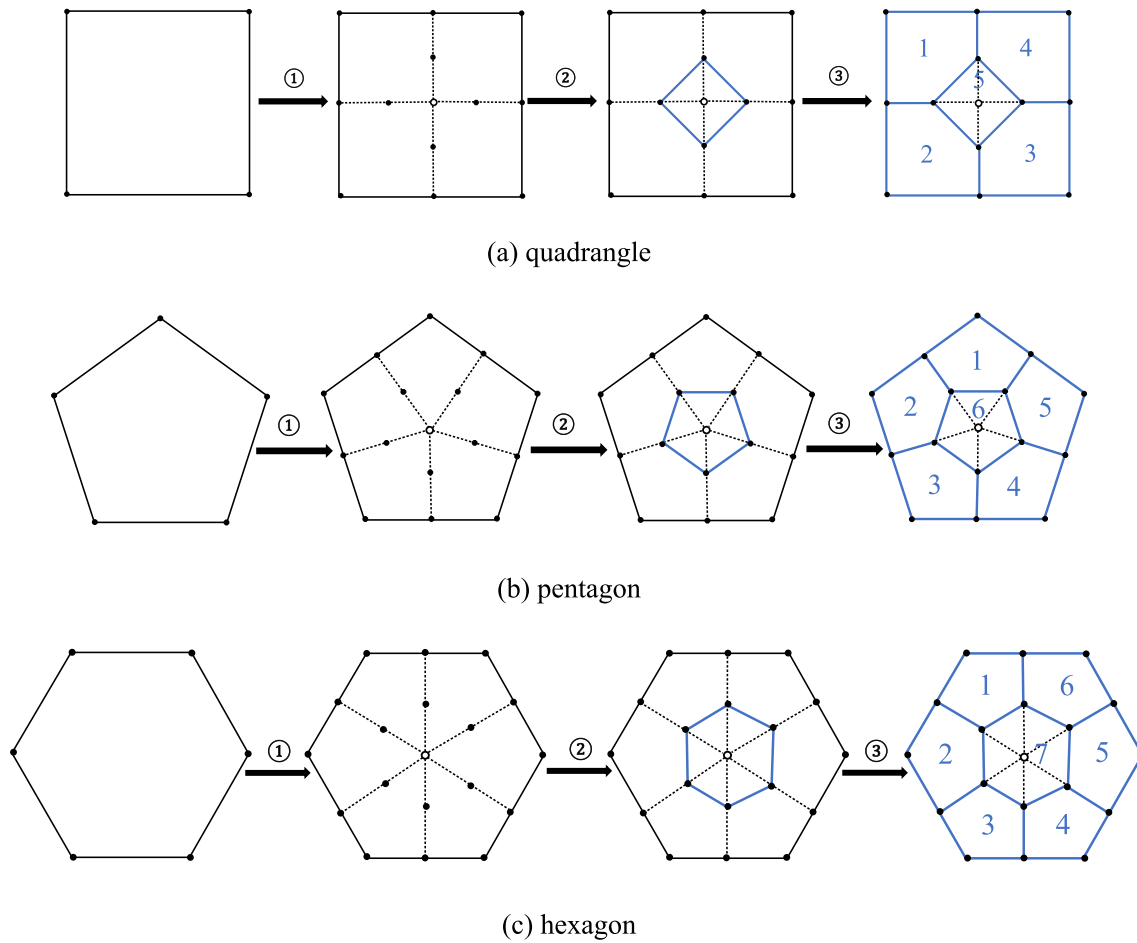


Fig. 2. Schematic diagrams of polytree refinement of standard polygons.

corresponding expression of the perfect elasto-plastic model is.

$$D_{ep} = D_e - \frac{D_e \left\{ \frac{\partial F}{\partial \sigma} \right\} \left\{ \frac{\partial F}{\partial \sigma} \right\}^T D_e}{A + \left\{ \frac{\partial F}{\partial \sigma} \right\}^T D_e \left\{ \frac{\partial F}{\partial \sigma} \right\}} \quad (2-17)$$

where D_e is the elastic constitutive matrix, and A is the plastic modulus.

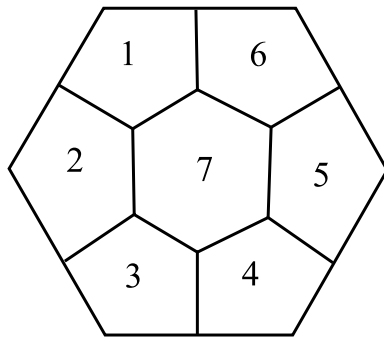
3. A flexible polytree-based mesh refinement algorithm

As we know, the computational precision in FE analysis generally depends on the mesh quality, the mesh refinement degree and so on. A coarse mesh can lead to unsatisfactory results (Elabbast et al., 2004), while extremely refined mesh for all over the finite element model requires high computational costs. In recent years, researches have been committed to using adaptive refinement technique to generate finite element mesh (Hirshikesh et al., 2020). Furthermore, owing to the presence and accumulation of the generalized shear strain/plastic strain, in fact, the occurrence of slope failure commonly just concentrates in a local region, which tends to occupy only a small proportion of the whole slope, thus it becomes necessary and meaningful to locally refine the mesh within the slope model. Therefore, in this section, we explore a flexible polytree-based mesh refinement algorithm to achieve the purpose of local mesh refinement.

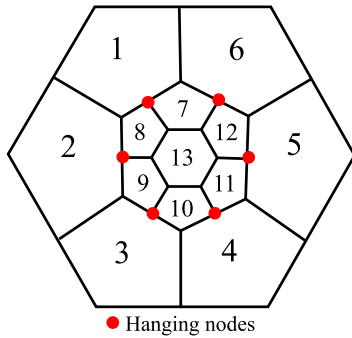
The quadtree decomposition technique can realize a rapid and efficient recursion in the process of mesh generation for conventional mesh shapes (Yerry and Shepard 1983; Tabarraei and Sukumar 2005), such as triangles and quadrangles. Inspired by the quadtree recursion approach, we adopt a novel polytree-based mesh refinement algorithm, which has got an initial application by Chau et al. (2017) and Nguyen et al. (2019),

to handle the slope stability problem. Following a certain recursion rule, the technique subdivides a polygon, called father element, into several children elements. More specifically, an ordinary polygon with n vertices is regularly subdivided into $(n + 1)$ sub-polygons, in which consists of a n -sided polygon located in the inside center position and n pentagons scattered around the radial direction, the whole refinement process can be expressed by the schematic diagram in Fig. 2, the number in the last step represents the newly generated element number. This process is called 1-level refinement. In the light of the requirement of the accuracy of analytical solution, the multistage mesh refinement process can be proceeded progressively until a satisfactory accuracy is achieved, Fig. 3 shows a group of polytree meshes after a 2-level refinement, the corresponding tree structure of 2-level refinement is depicted in Fig. 4.

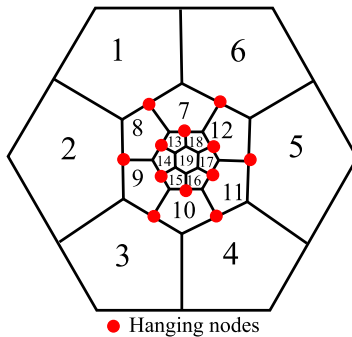
From Fig. 3, it is noteworthy that hanging nodes, denoted by red solid dots, appear at the intersection of different elements not located in the same refinement level after each refinement is completed. Since the incompatibility in calculating the hanging node displacement (Chen et al., 2018b; Zou et al., 2019), the traditional FE is a laborious and time-consuming avenue in dealing with the hanging node problem. However, based on the excellent performance of SBFEM, this difficulty can be successfully resolved through a conforming approximation field (Tabarraei and Sukumar 2007). In SBFEM, the n -sided polygon element with m hanging nodes is treated as a new polygon with $(n + m)$ vertexes. Through an iso-parametric mapping scheme, the element with hanging nodes can be regarded as a regular polygon (see Fig. 5), and the shape function of the new polygon element is naturally updated.



(a) initial mesh



(b) 1-level refined mesh



(c) 2-level refined mesh

Fig. 3. Polytree meshes with different level.

4. Strength reduction method (SRM)

SRM was first put forward by Zienkiewicz et al., (1975) in 1970 s and then has been widely applied in slope stability analysis by means of different research methods, such as the LE method (Cheng et al., 2007a) and the LA method (Li and Yang 2016). Additionally, the safety factor F_s is typically a preference for geotechnical researchers in the aspect of characterizing slope stability since it can not only manifest the stable state of the slope but predict the risk degree or safety of the slope. The essence of the SRM is to reduce the soil strength parameters by dividing “the strength reduction factor F_r ” until the soil fails, which is defined as follows.

$$c_d = c/F_r \quad (4-1)$$

$$\varphi_d = \arctan(\tan\varphi/F_r) \quad (4-2)$$

where c and φ are the cohesion and friction angle of soil, c_d and φ_d are the corresponding soil strength parameters after reduction. The F_r should gradually increase until the slope reaches a critical state. At this point, the current reduction factor F_r comes to be the safety factor F_s .

In the present work, combining the perfect elastic-plastic model following the Mohr-Coulomb criterion, SBFEM-SRM in slope stability analysis is carried out. This scheme avoids the shortcomings existed in some theoretical approaches based on the premise that the shape and location of the slope failure surface need to be predetermined, the limit state of slope can be determined by successive reduction, and thus to automatically trace the development and evolution of failure zone from local region to a fully connected generalized shear strain zone.

5. Slope failure criterion and local mesh refinement basis

Since the application of the SRM to slope stability analysis, several judgment criterions have been utilized to define the failure state of the slope, which generally comprise the following categories: (1) the non-convergence of the finite element solutions (Griffiths and Lane 1999; Dawson et al., 1999); (2) the displacement mutation of monitoring nodes (Tu et al., 2016; Ziekiewicz et al., 1975); (3) the full penetration of the generalized shear strain zone (Matsui and San 2008 ; Yao et al., 2017) or equivalent plastic strain zone (Zheng et al., 2009) from the toe

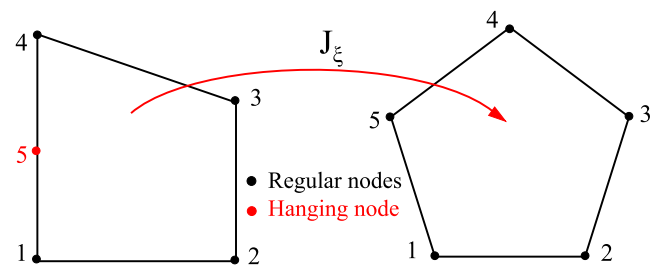


Fig. 5. Iso-parametric mapping over a polygon.

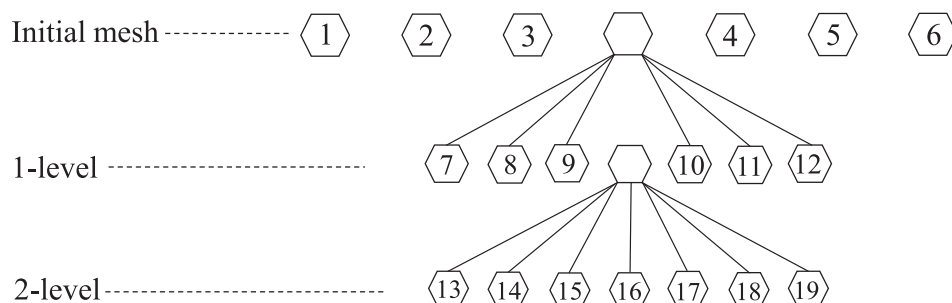


Fig. 4. Tree structure of a 2-level refinement.

to the crest of the slope. The above-mentioned three criteria keep a low percent error margin of safety factor (Zheng et al., 2009; Wu et al., 2018), and each criterion can achieve an ideal analysis outcome. Therefore, based on the implicit algorithm integrated into the finite element program GEODYNA developed by Zou et al., (2005), the displacement mutation criterion is adopted in the present work and taken as the criterion to judge the slope failure.

As the slope transforms to the instability state, a rapid accumulation and expansion of the generalized shear strain/equivalent plastic strain zone is also occurring simultaneously. Once the slope reaches the failure state, the strain zone can completely penetrate through the entire slope. It can be predicted that the critical failure surface of the slope should theoretically pass through the interior of the strain zone at which the greatest possibility of relative sliding of soil mass exists. However, as described in the previous section, the traditional theoretical approaches solving the critical failure surface need to make a prior assumption, this practice may lead to an overestimation of the safety factor (Khosravi and Khabbazi 2012). Conversely, the critical failure zone within a soil mass seems to be a better index for the slope failure (Khosravi and Khabbazi 2012). Therefore, instead of searching for a single critical failure surface, we could turn to determine the critical failure zone with the corresponding safety factor within the slope.

In this paper, in order to achieve a minimum computational cost, we use the flexible polytree-based mesh refinement algorithm to locally refine elements within the generalized shear strain zone. To distinguish elements for refinement, the generalized shear strain ε_g is used as a refinement indicator to locate elements among the whole elements in refinement process. Specifically, this strategy is to start SBFEM-SRM calculation from an initially coarse analysis mesh, which could be called “initial mesh”, to form a relatively vast shear strain zone. Ulteriorly, the generalized shear strain value ε_g over each element is managed to conduct mesh refinement, and a refinement threshold ε_a is defined, which selects an appropriate value based on the ε_g value derived from “initial mesh”. The refinement threshold is used to automatically filtered out a set of elements, which have smaller shear strain values than the refinement threshold, such that.

$$\varepsilon_{gi} \leq \varepsilon_a, \quad i \leq n \quad (5-1)$$

$$\varepsilon_{gi} = \frac{\sqrt{2}}{3} \left[(\varepsilon_{ix} - \varepsilon_{iy})^2 + \varepsilon_{ix}^2 + \varepsilon_{iy}^2 + \frac{3}{2} \gamma_{ixy}^2 \right] \quad (5-2)$$

where ε_{gi} is the generalized shear strain value of i -th element, n is the number of elements, and ε_{ix} , ε_{iy} and γ_{ixy} are the strain components of the i -th element respectively. Therefore, the minimal set Ω_{min} and the maximum set Ω_{max} are thus determined. Subsequently, the mesh is refined adaptively by using polytree-based mesh refinement algorithm in zones contained in the maximum set Ω_{max} characterized by higher shear strain values, the new mesh is called “1-level refined mesh”. Similarly, it's conceivable that the SBFEM-SRM calculation with “1-level refined mesh” tends to obtain a narrower shear strain zone than “initial mesh”. Thereafter, the procedure of local mesh refinement could be recursive once. Thus, the bandwidth of shear strain zone is bound to be forced to a limited space after multistage mesh refinement, and then the approximate path of the failure surface can be easily traced.

6. Numerical example verifications

In this section, in order to verify the dependability and the applicability of the proposed method in terms of SBFEM-SRM and polytree-based polygonal mesh refinement algorithm, the numerical simulation of polygonal discretization is conducted to evaluate the slope stability. The numerical algorithm discussed in the previous section is implemented in the independently developed finite element program GEODYNA. This section consists of three subsections: The calculational accuracy and superiority of SBFEM-SRM are firstly verified using a

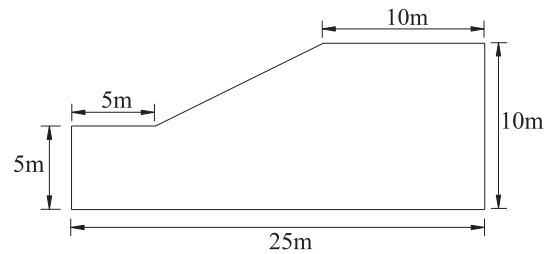


Fig. 6. The geometry of the slope of Example 1.

Table 1

Material parameters of filling soil.

c/kPa	$\varphi/(^{\circ})$	$\gamma/(\text{KN}/\text{m}^3)$	E/MPa	ν
9.8	10	17.64	0.1	0.3

simple slope example. Second, through a nonhomogeneous slope example with complex geological conditions, the proposed method in terms of SBFEM-SRM in conjunction with polytree-based polygonal mesh refinement algorithm in slope stability analysis is demonstrated. Third, an actual test embankment example is analyzed to verify the practicability of the proposed method.

Both safety factor and the generalized shear strain zone are used to characterize the slope stability performance. In particular, the numerical results obtained by the proposed method are compared with available analytical solutions from other existing solutions for verification purpose. Details of this section are showed as below.

6.1. Example 1-Simple homogeneous slope

6.1.1. Model and material parameters

In this section, a classical homogeneous slope called Example 1 is selected to evaluate the correctness and advantage of the SBFEM-SRM. It is a simple 20 m high slope with an inclination of 1:2, the geometry of the slope is depicted in Fig. 6. The behavior of filling soil conforms to a perfect elasto-plastic model following the Mohr-Coulomb criterion incorporating non-associated flow rule, a value of dilatancy angle $\psi = 0^{\circ}$ is assumed, which has been proved to be reliable in RSM analysis by Griffiths and Line (1999). Horizontal node displacements along the left and right boundaries are fixed, and all node displacements along the bottom boundary are fixed, while the top surface of model keeps free. The related soil parameters friction angle φ , cohesion c , self-weight γ , elastic modulus E , and Poisson's ratio ν are listed in Table 1. Besides, the soil is completely dry and impervious to groundwater.

In the initial stress stage, the self-weight of soil is taken into consider. soil is assumed to be an elastic material. The lateral earth pressure coefficient at rest K_0 is defined with $K_0 = 1 - \sin\varphi$ according to Jaky (1944), so Poisson's ratio ν can be obtained by the generalized Hooke's law: $\nu = K_0/(1 + K_0)$. The elastic modulus E is consistent with the values in Table 1, the SBFEM analysis is then performed to generate the initial stress under its self-weight. After that, the initial stress is introduced into the strength reduction calculation process of SBFEM to gradually obtain

Table 2

Different element types used in Example 1.

Name	Shape	Number of nodes
Quadrilateral isoparametric element (Quad4)		4
Quadratic isoparametric element (Quad8)		8
Linear Polygon element (LP)		n ($n = 3, 4, 5, \dots$)

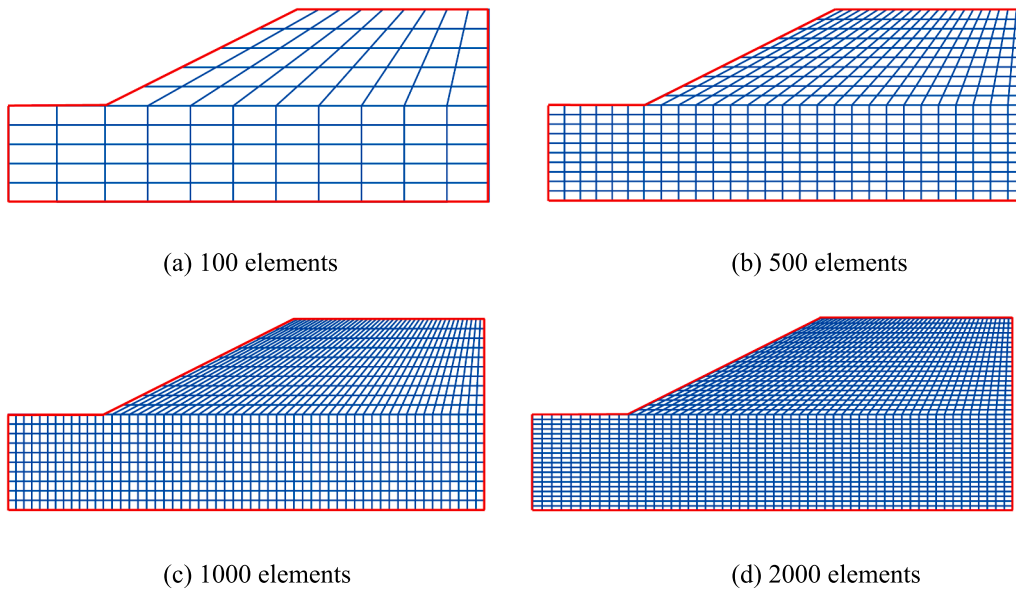


Fig. 7. Quadrilateral elements divisions.

the critical state of the slope.

6.1.2. Analytical options

6.1.2.1. FE-SRMxxx. Based on Example 1, firstly, the conventional FE-SRM analysis is carried out to conduct the slope stability analysis, the soil parameters required in the simulation are shown in Table 1. The isoparametric quadrilateral elements with 4 nodes (Quad4) and 8 nodes (Quad8), see Table 2, are used to conduct the FE analysis. For presentation purposes, the FE-SRM analysis program by using Quad4 and Quda8 elements, has been abbreviated as FE-SRM-Q4 and FE-SRM-Q8 separately.

6.1.2.2. SBFEM-SRMxxx.

(1) Quadrilateral elements

In order to demonstrate the accuracy and reliability of SBFEM-SRM in slope stability analysis, regarding the slope example in FE-SRM analysis of Section 6.1.2.1, the presented SBFEM-SRM is also performed, and quadrilateral elements are used in this section, which can be abbreviated as SBFEM-SRM-Q4. The mesh Information and soil parameters are consistent with Section 6.1.2.1.

(2) Linear Polygon elements

In addition to being able to calculate regular cells. The proposed method in terms of SBFEM-SRM can also support the polygonal elements and derive high-precision solution, which is its distinguishing feature from the conventional FE-SRM analysis. In order to further verify the superiority and applicability of the proposed method, combined with linear polygon elements (LP), offered in Table 2, the studied slope model in above analyses is further investigated, and for comparison purposes, the scheme is designated as SBFEM-SRM-LP.

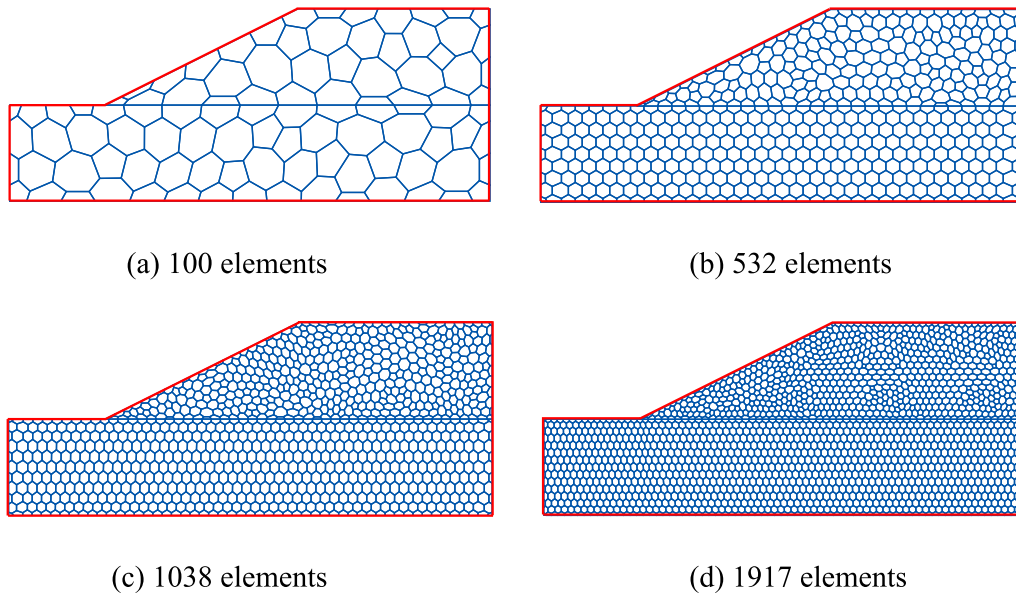


Fig. 8. Polygonal elements divisions.

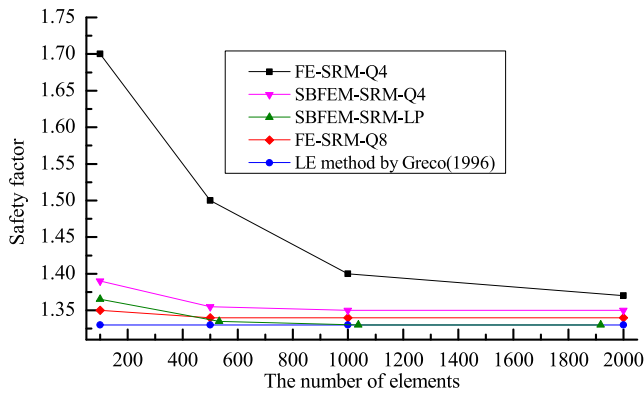


Fig. 9. Safety factor of different element types for different element numbers.

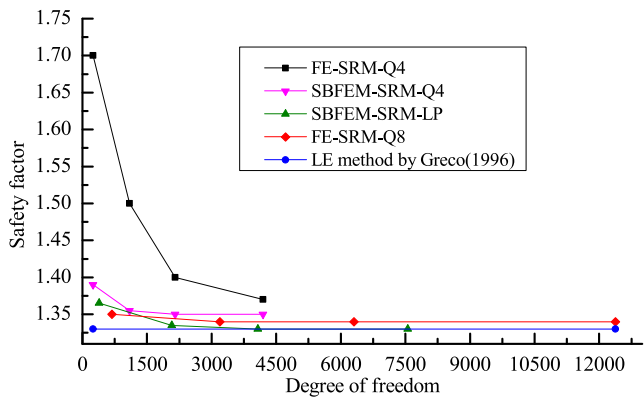


Fig. 10. Safety factor of different element types for different degrees of freedom.

6.1.3. Mesh information

(1) Quadrilateral elements

The slope model is discretized into meshes with 100, 500, 1000 and 2000 quadrilateral elements respectively, see Fig. 7. For Quad4 element, the number of nodes is 122, 549, 1077 and 2096, while 343, 1579, 3153 and 6191 nodes for Quad8 element respectively. Based on this meshing, the numerical analysis of FE-SRM-Q4, FE-SRM-Q8 and SBFEM-SRM-Q4 are carried out successively. The safety factor F_s for different element numbers and degrees of freedom are obtained to serve as the evaluation index of slope stability.

(2) Polygonal elements

Similarly, the slope model is discretized into a mesh with 100, 532, 1038 and 1912 polygon elements, see Fig. 8, which has an approximate number of elements as the previous content. The corresponding number of nodes is 193, 1039, 2037 and 3779. Then the SBFEM-SRM-LP analysis is implemented.

6.1.4. Results for simple slope

(1) FE-SRM-Q4 and FE-SRM-Q8

The relationship curves between the error of FE-SRM-Q4 and FE-SRM-Q8 with different element numbers are shown in Fig. 9, the influence of degrees of freedom, corresponding to the number of elements in Fig. 9, on the safety factor is shown in Fig. 10. To clearly show the difference of FE-SRM results with other method, the value for LE method

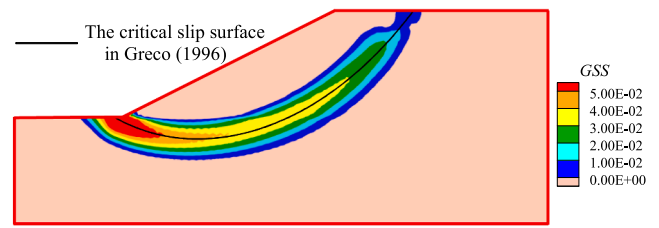


Fig. 11. The critical failure zone for SBFEM-SRM of polygonal elements.

by Greco (1996) is also included in the graphs. From the results, it is clear that the calculation accuracy of FE-SRM-Q8 is hardly affected by element numbers and degrees of freedom, and its accuracy is much better than that of FE-SRM-Q4, meanwhile, the safety factors obtained from the FE-SRM-Q8 keeps good consistency with the analytical solutions obtained from LE method, implying that FE-SRM-Q8 offers ideal computing reliability in solving the safety factor of slope. This is mainly attributed to the fact that Quad8 has more degrees of freedom under the same number of elements, which contributes to the robustness of the calculation results. However, the calculation results of FE-SRM are not very satisfactory when Q4 elements are used, especially in the case of a coarse mesh density.

(2) SBFEM-SRM-Q4

The safety factors obtained from SBFEM-SRM-Q4 for different element number and freedom degrees are illustrated in Fig. 9 and Fig. 10. Compared with the curves of FE-SRM-Q4, the curves of SBFEM-SRM-Q4 are obviously closer to the theoretical value which is regarded as the value of LE method. Besides, note that the curves of SBFEM-SRM-Q4 vary slightly with the mesh density and freedom degrees, indicating SBFEM-SRM has better mesh adaptability. These results confirm that SBFEM has better computational accuracy than FE in slope stability analysis.

(3) SBFEM-SRM-LP

The variation trend of safety factor with mesh density and freedom degree obtained from SBFEM-SRM-LP is also shown in the curve in Fig. 9 and Fig. 10. As shown in the figures, the results obtained from SBFEM-SRM-LP are obviously more accurate than those obtained from SBFEM-SRM-Q4, which shows that polygonal elements have better computational accuracy than quadrilateral elements. In addition, with the increase of mesh density and freedom degree, the curves of SBFEM-SRM-LP change slightly and the general trends are very close to the curves of FE-SRM-Q8, the values of the two curves also differ very slightly. In addition, it should be noted that the degree of freedom of SBFEM-SRM-LP is less than that of FE-SRM-Q8, but the calculation accuracy is not weakened, which proves the accurate calculation ability of SBFEM compared with FE method. In other words, the calculation accuracy of SBFEM-SRM-LP is enough to reach the accuracy of FE-SRM-Q8.

The critical failure zone characterized by generalized shear strain (GSS) obtained from the SBFEM-SRM-LP corresponding to 1917 elements is depicted in Fig. 11, and the critical slip surface located in Greco (1996) by LE method is also contained. Intuitively, the critical failure zone formed by SBFEM-SRM-LP also accurately trace the approximate path of the critical slip surface in Greco (1996). The phenomenon illustrates that the proposed method is also capable of capturing critical failure zone of slope with high precision. These capabilities of SBFEM-SRM will be a particular important feature in problems that cannot be solved by LE and LA methods, such as complex terrain and loading conditions.

Although the calculation accuracy of FE-SRM-Q8 is comparable to that of SBFEM-SRM-LP, the calculation process of Q8 element is time-consuming, and there will be an additional difficulty in multistage

Table 3Safety factors of slope for different ψ in Example 1.

$\psi/^\circ$	0	3	6	9
F_s	1.330	1.335	1.340	1.346

mesh refinement. Therefore, in contrast, SBFEM-SRM-LP adopted in this paper is undoubtedly a better choice for slope stability analysis.

In general, the advancement of the proposed method in computational accuracy and effectiveness has been significantly demonstrated through this example.

6.1.5. The influence of dilatancy angle on results

6.1.5.1. Dilatancy angle parameters. In the above section, the non-associated flow rule with dilatancy angle $\psi = 0^\circ$ is adopted. In order to examine the influence of ψ on the calculation results, several SBFEM-SRM calculations by varying ψ , which corresponds to 3° , 6° and 9° respectively, are performed.

6.1.5.2. The effects of ψ on safety factor. The obtained safety factors are listed in Table 3. As can be seen from Table 3, with the increase of ψ , the safety factor presents an increasing trend, it shows the dilatancy angle has a slight effect on slope stability. The error between the safety factor of $\psi = 0^\circ$ and that of $\psi = 9^\circ$ is 1.20%, which confirms that the effect of ψ on the safety factor is insignificant and less important in SRM. The insensitivity of slope stability to dilatancy angle in SRM is also confirmed by Cheng et al. (2007a) and Liu et al. (2015a) through some numerical examples.

6.1.5.3. The effects of ψ on critical failure zone. The corresponding contours of critical failure zone for $\varphi = 10^\circ$ corresponding to different dilatancy angles are shown in Fig. 12 respectively. According to the contours of critical failure zone, it can be seen the change of dilatancy angle has no significant influence on the critical failure zone of slope. In fact, the width of this zone is mainly affected by the mesh density which is also the issue this study is committed to solve.

In addition, as described in Griffiths and Lane (1999), slope stability analysis is relatively unconfined, so the choice of dilation angle is less important, a compromise value of $\psi = 0^\circ$, which is also adopted in this

study, enables the model to give reliable safety factors and reasonable indication of the potential failure surfaces. Therefore, the selection of $\psi = 0^\circ$ is applicable to the slope cases investigated by this study, for slopes subjected to confining pressure, matrix suction etc. (Guo et al., 2010; Hossain and Yin, 2015), the value of dilatancy angle should be further studied.

6.2. Example 2- a nonhomogeneous slope

In this section, the flexibility and feasibility of SBFEM-SRM combined with the polytree-based polygonal mesh refinement algorithm in slope with complex geological conditions are examined. A multilayered nonhomogeneous slope composed of three different soils, called Example 2, is considered, parameters of three soils following a non-associated Mohr-Coulomb failure criterion with $\psi = 0^\circ$ are listed in Table 4. The initial stress generation process, boundary and ground-water conditions are consistent with those in Example 1. Fig. 13 shows the geometric shape of the slope.

This slope is a representative analysis example investigated by association for computer aided designs (ACADS) (Donald and Giam 1992). In order to obtain more reliable results, many excellent researchers and research institutions were invited to engage in this case study (Hou et al., 2017), and different research methods have been developed, among which the most important one is LE method.

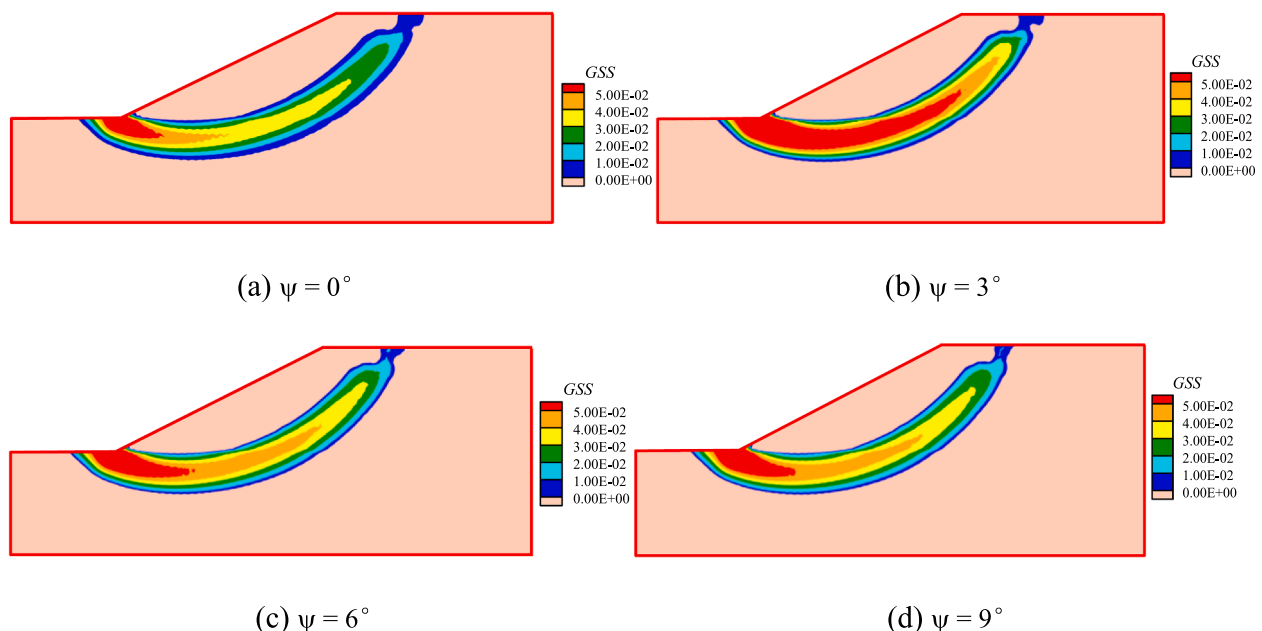
6.2.1. LE method

In the framework of the LE method, researchers have solved the safety factor of the slope by means of different optimization methods or algorithms, several F_s values obtained by different methods from different literatures are summarized in Table 5, in which the safety factor values range from 1.35 to 1.39. In addition, the shape and position of the critical slip surface obtained by these methods remain roughly

Table 4

Parameters of the three soils.

Soil	c/kPa	$\varphi/^\circ$	$\gamma/(\text{KN}/\text{m}^3)$	E/MPa	ν
Layer 1	0	38	19.5	0.1	0.3
Layer 2	5.3	23	19.5	0.1	0.3
Layer 3	7.2	20	19.5	0.1	0.3

**Fig. 12.** The critical failure zone for different ψ in Example 1.

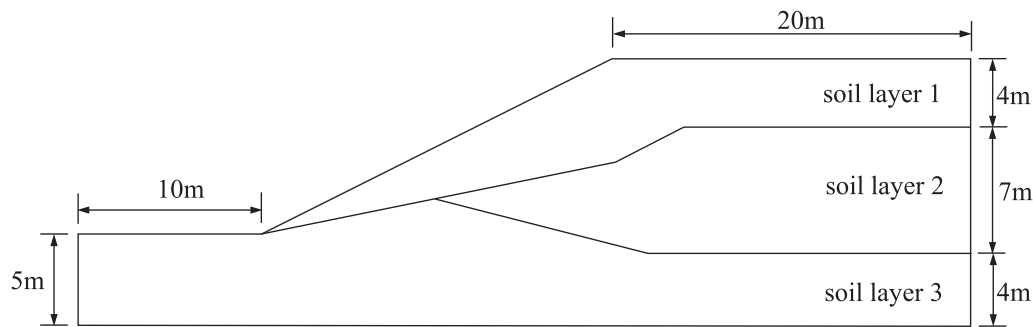


Fig. 13. The geometric shape of the Example 2.

Table 5

F_s obtained from different methods for Example 2.

Source	Method	Safety factor F_s
Gao (2016)	Ant-colony optimization	1.344
Cheng et al., (2007b)	Harmony search algorithm	1.387
Bolton et al., (2003)	Leap-frog	1.359
Goh (1999)	Genetic algorithm	1.387

similar.

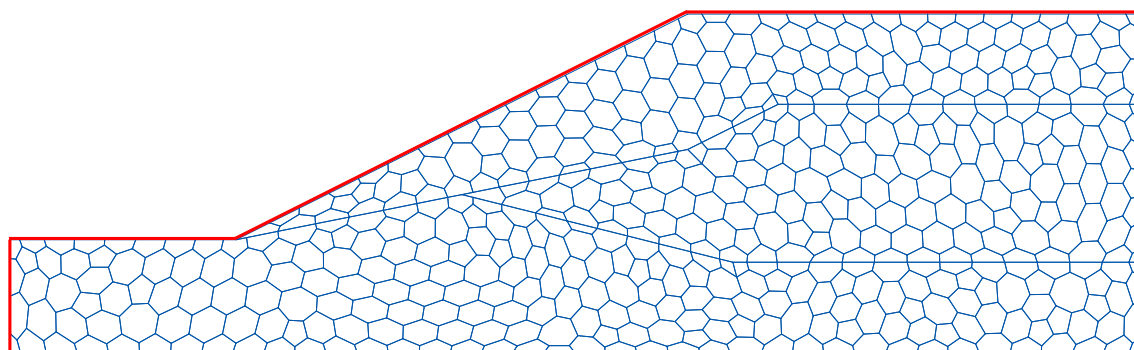
6.2.2. SBFEM-SRM analysis of flexible polygonal mesh refinement algorithm

In this section, the flexible polytree-based polygonal mesh refinement algorithm proposed in this paper is verified. First, based on Example 2, the slope model is initially discretized into a coarse mesh with 498 polygonal elements in our simulation, see Fig. 14(a). Then, SBFEM-SRM is carried out to search for the limit state of the

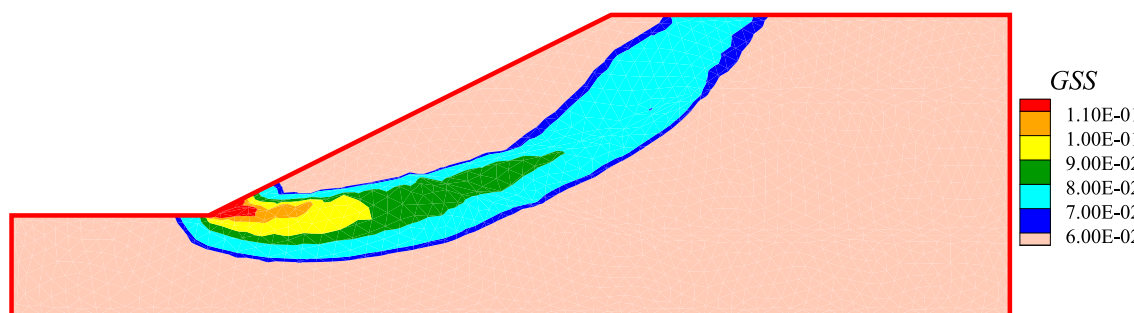
nonhomogeneous slope, during which the critical failure zone corresponding to the safety factor can be formed. After the simulation analysis, the safety factor F_s is 1.430 in the limit state, and the critical failure zone, which is represented by generalized shear strain (GSS), is simultaneously identified and shown in Fig. 14(b).

In order to demonstrate the advantage of polygonal mesh refinement algorithm, after the above analysis process, the independently developed polytree-based mesh refinement algorithm, which can automatically implement and finally realize the multistage local mesh refinement to improve the calculation accuracy of the slope, is introduced into SBFEM-SRM. During the refinement process, the physical mesh attains 4012 polygonal elements after the 2-level refinement in this example, as exhibited in Fig. 15(a). The solved critical failure zone is depicted in Fig. 15(b).

It can be found from the figure that as the mesh is improved from initial mesh to 2-level refined mesh, the critical failure zone achieves a large area reduction, and the zone in 2-level refined mesh will be gathered towards inner elements in the initial coarse mesh. Therefore,

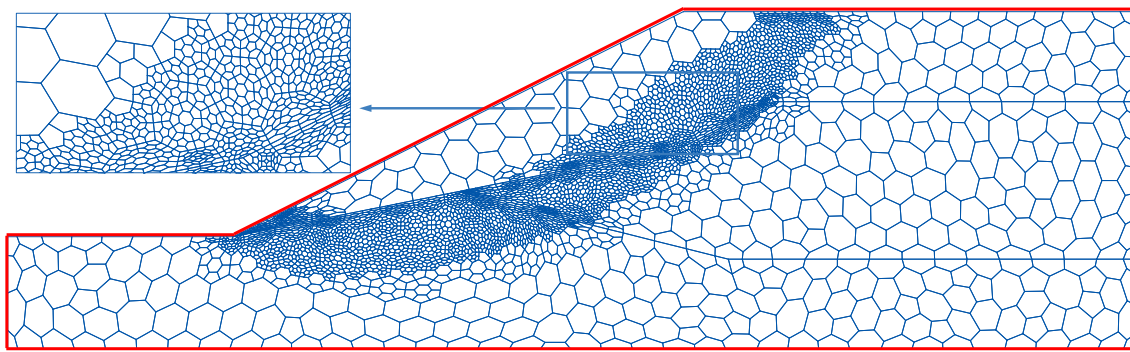


(a) Mesh

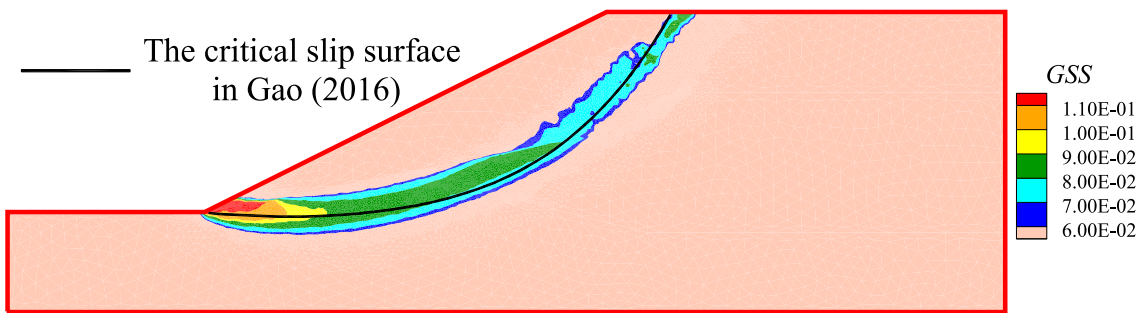


(b) The critical failure zone

Fig. 14. SBFEM-SRM of initial mesh for Example 2.



(a) Mesh



(b) The critical failure zone

Fig. 15. SBFEM-SRM of 2-level mesh for Example 2.

the proposed method also realizes the target in critical failure zone reduction of slope with complex geological structure. Gao (2016) analyzed the slope using the ant colony optimization method, the optimum critical slip surface is depicted in Fig. 15(b). Evidently, the critical failure zone obtained by the proposed method has already accomplished the function of completely enclosing the optimum critical slip surface, thus the determined critical failure zone can exactly capture the path of the theoretical critical slip surface of the nonhomogeneous slope. The safety factor F_s corresponding to 2-level mesh is 1.392, which is slightly

larger than the upper bound value 1.387 of F_s in Table 5, with a discrepancy of 0.22%, while the premise in terms of the shape and location of the slope failure surface in theoretical optimization algorithm is eliminated. In addition, safety factors exhibit a decreasing tendency with the improvement of mesh level, such as 1.430 for initial mesh and 1.392 for 2-level refined mesh. The phenomenon of the decrease of safety factor is in line with the rule that a finer mesh contributes to a more exact solution. Finally, it can be seen from Fig. 15(a) that a large number of hanging nodes have generated in the refinement

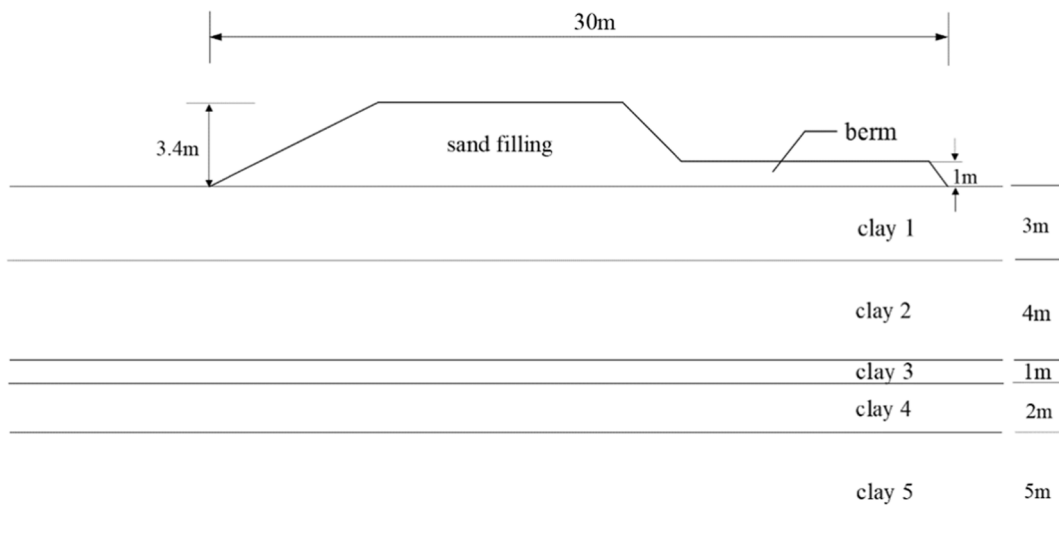


Fig. 16. The cross-section diagram of Example 3.

Table 6
Soil parameters for Example 3.

layer	$\gamma/(\text{kN}\cdot\text{m}^{-3})$	C_u/kPa	$\varphi/^\circ$	E_u/MPa	ν_u
sand filling	18.0	0	37.5	30.0	0.3
Bangkok clay 1	14.3	13.3	0	20.0	0.495
Bangkok clay 2	14.3	10.5	0	20.0	0.495
Bangkok clay 3	14.3	13.3	0	20.0	0.495
Bangkok clay 4	15.0	17.5	0	20.0	0.495
Bangkok clay 5	16.0	21.0	0	20.0	0.495

process, and the SBFEM-SRM adopted in this paper deals with them ingeniously and reliable results are obtained.

6.3. Example 3- a full-scale trial embankment

To examine the practicability and applicability of the SBFEM-SRM combined with the flexible polytree-based polygonal mesh refinement algorithm in slope stability analysis, a full-scale trial embankment called Example 3 built at Nong Ngoo Hao in Bangkok by the Asian Institute of Technology (Zou et al., 1995; Zhu, 2001) is simulated in this section. The simplified cross-section and soil layer distribution of the test embankment are given in Fig. 16. The embankment was 30 m long with side slopes of 1:2 (vertical: horizontal), a berm was constructed on one side to ensure that failure occurred on the opposite side. The embankment built on Bangkok clay collapsed at a height of approximately 3.4 m.

For the sand filling material, a set of characteristic parameters, listed in Table 6, was obtained from laboratory tests (Zou et al., 1995; Bergado et al., 1987). Bangkok clay is divided into 5 horizontal layers with characteristic properties of the different soil deposits and the partition of each layer is shown in Fig. 16. The soil parameters required in this analysis are summarized in Table 6. The undrained shear strengths of Bangkok clay, C_u were estimated from field vane tests and have been

corrected using Bjerrum's correction factor (Bjerrum, 1972). The undrained Young's modulus (E_u) of Bangkok clay was determined from the cone penetration test results, and the undrained Poisson's ratio ν_u was assumed to be 0.495 (Zou et al., 1995). The initial stress generation process, boundary conditions, groundwater conditions and flow rule of soils in this example are also consistent with those in Example 1.

Based on the example, SBFEM-SRM analysis combined with the polytree-based polygonal mesh refinement algorithm is conducted in this section. The slope model is initially discretized into a coarse mesh with 1132 polygonal elements in our simulation, see Fig. 17(a). Then SBFEM-SRM is carried out to search for the limit state of the slope, and the safety factor F_S is 1.070 in the limit state, the corresponding critical failure zone is shown in Fig. 17(b). Further, the multistage local mesh refinement process and SBFEM-SRM are continued in parallel.

After the 2-level refinement process, the slope mesh attains 5512 polygonal elements as exhibited in Fig. 18(a). The safety factor F_S is 1.045 in the limit state, and the solved critical failure zone is depicted in Fig. 18(b). By comparing Fig. 17(b) with Fig. 18(b), it can be found that as the mesh refinement level improves, the zone shows a tendency of sharp shrinkage. Therefore, the proposed local mesh refinement algorithm indeed achieves the desired purpose in critical failure zone reduction for this embankment slope. Notably, there was six failure points observed in the field as shown in Fig. 18(b), the determined failure band passes through all the six observed failure points. In the light of this we could identify that the proposed method provides a good conformity with the actual failure surface. Besides, the safety factor 1.045 obtained by SBFEM-SRM is slightly larger than the value of 1.0 in the theoretical limit state, the error may result from the uncertainty of soil strength measurements and realistic construction situation, the safety factor cannot exactly be identical with the theoretical solution 1.0. In terms of practical engineering, such an error could be reasonably accepted.

Therefore, the proposed method provides good performance and

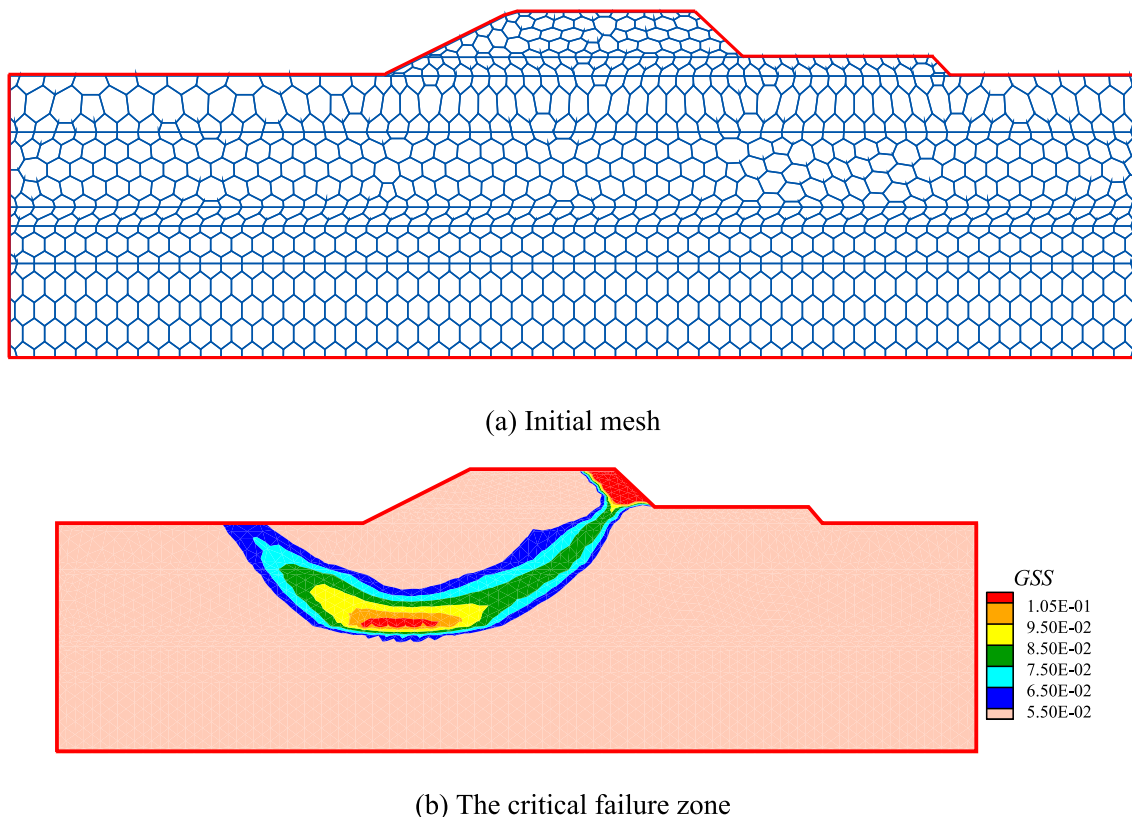


Fig. 17. SBFEM-SRM of initial mesh for Example 3.

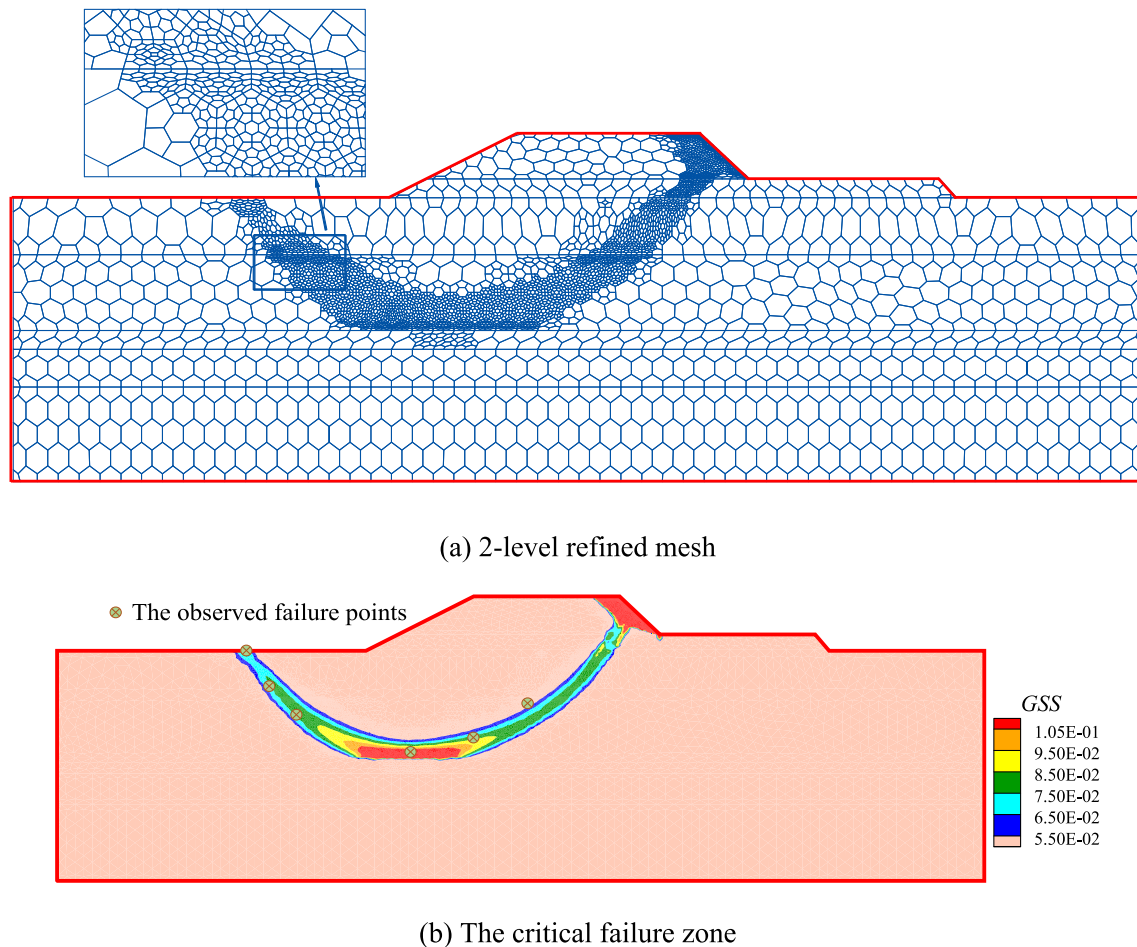


Fig. 18. SBFEM-SRM of 2-level mesh for Example 3.

applicability in practical engineering, the further application can be assigned to a wider range of slope engineering to provide theoretical basis for its construction and design.

It is worth noting that the above studied examples all focus on ideal elastic–plastic soil materials which ignores the strain-softening effect of soil. Within the framework of SBFEM, damage failure of materials, which is one of the strain-softening property, has been successfully analyzed by relevant studies (e.g. Zhang et al., 2018; Chen et al., 2019; Gong et al., 2021) and corresponding conclusions have been achieved. Therefore, it has proven that SBFEM has a very robust ability and versatility in dealing with strain-softening problem. As for elastic–plastic soil materials considering strain-softening characteristics, the related research on the combination of SBFEM and local mesh refinement algorithm may be developed and discussed in the future research.

7. Conclusion

In this paper, a fresh slope stability analysis approach and application is investigated. Specifically, a flexible polytree-based mesh refinement algorithm has been developed independently to overcome the limitation of conventional methods, making a local refinement and scale spanning of the mesh can be achieved efficiently. Meanwhile, combined the scaled boundary finite element method and strength reduction method, a refinement analysis method for slope stability has been established. Subsequently, several examples are analyzed to verify the accuracy and applicability of the proposed method. The main conclusions are listed as follows:

- (1) The advantages of SBFEM and SRM have been inherited in the proposed method, and specific characteristics can be embodied as: Firstly, flexible polygonal elements can be solved directly in slope stability analysis, making the efficiency for processing complex geometries improved. And the flexible polytree-based mesh refinement algorithm can be coupled seamlessly, so that multistage refinement can be performed conveniently. In addition, the safety factor and the generalized shear strain can be obtained simultaneously, which has served as the evaluation indexes of slope stability.
- (2) A highly satisfactory solution accuracy is achieved in the proposed approach, wherein obtained results are in good agreement with other theoretical solutions offered in literatures, implying that a very superb validity and applicability for numerical analysis is revealed. Particularly, as the calculations indicated, polygonal elements have a remarkable advantage of high precision for slope stability analysis, in that the calculation results of SBFEM-SRM-LP can achieve the accuracy comparable to FE-SRM-Q8. Meanwhile, the difficulties existing in multistage mesh refinement of Q8 elements would be eliminated via presented method, and the hanging node problem can be dealt with reasonably to ensure the compatibility and conformity of computation.
- (3) Compared to conventional methods, the presented refinement algorithm can offer a more desired solution without compromising the solution accuracy, and the majority unnecessary computational burden can be retrenched. In particular, the advantage would be better revealed when the method is extended

to 3D analysis, which will be a major research object for us in the future.

CRediT authorship contribution statement

Xiupeng Nie: Investigation, Software, Data curation, Writing – original draft. **Kai Chen:** Methodology, Validation, Writing – review & editing. **Degao Zou:** Conceptualization, Funding acquisition, Supervision. **Xianjing Kong:** Resources, Supervision. **Jingmao Liu:** Software, Validation. **Yongqian Qu:** Methodology, Validation.

Declaration of Competing Interest

The authors declare that they have no known competing financial interests or personal relationships that could have appeared to influence the work reported in this paper.

Acknowledgements

This work was supported by the National Natural Science Foundation of China (Grant Nos. 52192674, U1965206, 52009018) and the Fundamental Research Funds for the Central Universities (Grant Nos. DUT21RC(3)099).

References

- Ausilio, E., Conte, E., Dente, G., 2000. Seismic stability analysis of reinforced slopes. *Soil. Dyn. Earthq. Eng.* 19 (3), 159–172. [https://doi.org/10.1016/S0267-7261\(00\)00005-1](https://doi.org/10.1016/S0267-7261(00)00005-1).
- Bergado, D.T., Miura, N., Chang, J.C., Danzuka, M., 1987. Reliability assessment of test embankments on soft Bangkok clay by variance reduction and nearestneighbour methods. *Comput. Geotech.* 4 (3), 171–194. [https://doi.org/10.1016/0266-352X\(87\)90046-2](https://doi.org/10.1016/0266-352X(87)90046-2).
- Bjerrum, L., 1972. Embankments on soft ground. Performance of Earth and Earth-Supported Structures.
- Bolton, H.P.J., Heymann, G., Groenwold, A., 2003. Global search for critical failure surface in slope stability analysis. *Eng. Optimiz.* 35 (1), 51–65. <https://doi.org/10.1080/0305215031000064749>.
- Byfut, A., Schroeder, A., 2017. Unsymmetric multi-level hanging nodes and anisotropic polynomial degrees in H^1 -conforming higher-order finite element methods. *Comput. Math. Appl.* 73 (9), 2092–2150. <https://doi.org/10.1016/j.camwa.2017.02.029>.
- Chau, K.N., Chau, K.N., Ngo, T., Hackl, K., Nguyen, X.H., 2017. A polytree-based adaptive polygonal finite element method for multi-material topology optimization. *Comput. Method. Appl. M.* 332, 712–739. <https://doi.org/10.1016/j.cma.2017.07.035>.
- Chen, K., Zou, D.G., Kong, X.J., 2017a. A nonlinear approach for the three-dimensional polyhedron scaled boundary finite element method and its verification using Koyna gravity dam. *Soil. Dyn. Earthq. Eng.* 96, 1–12. <https://doi.org/10.1016/j.soildyn.2017.01.028>.
- Chen, K., Zou, D.G., Kong, X.J., Chan, A., Hu, Z.Q., 2017b. A novel nonlinear solution for the polygon scaled boundary finite element method and its application to geotechnical structures. *Comput. Geotech.* 82, 201–210. <https://doi.org/10.1016/j.compgeo.2016.09.013>.
- Chen, K., Zou, D.G., Kong, X.J., Yu, X., 2018a. An efficient nonlinear octree SBFEM and its application to complicated geotechnical structures. *Comput. Geotech.* 96, 226–245. <https://doi.org/10.1016/j.compgeo.2017.10.021>.
- Chen, K., Zou, D.G., Kong, X.J., Zhou, Y., 2018b. Global concurrent cross-scale nonlinear analysis approach of complex CFRD systems considering dynamic impervious panel-rockfill material-foundation interactions. *Soil. Dyn. Earthq. Eng.* 114, 51–68. <https://doi.org/10.1016/j.soildyn.2018.06.027>.
- Chen, K., Zou, D., Kong, X., Liu, J., 2019. Elasto-plastic fine-scale damage failure analysis of metro structures based on coupled SBFEM-FEM. *Comput. Geotech.* 108, 280–294. <https://doi.org/10.1016/j.compgeo.2018.12.030>.
- Chen, K., Zou, D.G., Tang, H.X., Liu, J.M., Zhuo, Y., 2021. Scaled boundary polygon formula for Cosserat continuum and its verification. *Eng. Anal. Bound. Elem.* 126, 136–150. <https://doi.org/10.1016/j.enganabound.2021.02.007>.
- Cheng, Y.M., Lansivaara, T., Wei, W.B., 2007a. Two-dimensional slope stability analysis by limit equilibrium and strength reduction methods. *Comput. Geotech.* 34 (3), 137–150. <https://doi.org/10.1016/j.compgeo.2006.10.011>.
- Cheng, Y.M., Li, L., Chi, S.C., 2007b. Performance studies on six heuristic global optimization methods in the location of critical slip surface. *Comput. Geotech.* 34 (6), 462–484. <https://doi.org/10.1016/j.compgeo.2007.01.004>.
- Chi, H., Talisch, C., Lopez-Pamies, O., H. Paulino, G., 2015. Polygonal finite elements for finite elasticity. *Int. J. Numer. Methods. Engrg.* 101 (4), 305–328. <https://doi.org/10.1002/nme.4802>.
- Cramer, H., Rudolph, M., Steinl, G., Wunderlich, W., 1999. A hierarchical adaptive finite element strategy for elastic-plastic problems. *Comput. Struct.* 73 (1–5), 61–72. [https://doi.org/10.1016/S0045-7949\(98\)00268-5](https://doi.org/10.1016/S0045-7949(98)00268-5).
- Dawson, E.M., Roth, W.H., Drescher, A., 1999. Slope stability analysis by strength reduction. *Geotechnique* 49 (6), 835–840. <https://doi.org/10.1680/geot.1999.49.6.835>.
- Donald, I.B., Giam, P.S.K., 1992. Soil slope stability programs review. Association for Computer Aided Design, Melbourne, Australia.
- Elabbasi, N., Hong, J.-W., Bathe, K.-J., 2004. On the reliable solution of contact problems in engineering design. *Int. J. Mech. Mater.* 1 (1), 3–16. <https://doi.org/10.1023/B:MAMD.0000035458.72478.7a>.
- Gao, X., Liu, H., Zhang, W., Wang, W., Wang, Z., 2019. Influences of reservoir water level drawdown on slope stability and reliability analysis. *GEORISK*. 13 (2), 145–153. <https://doi.org/10.1080/17499518.2018.1516293>.
- Gao, W., 2016. Determination of the noncircular critical slip surface in slope stability analysis by meeting ant colony optimization. *J. Comput. Civil. Eng.* 30 (2), 06015001. [https://doi.org/10.1061/\(ASCE\)CP.1943-5487.0000475](https://doi.org/10.1061/(ASCE)CP.1943-5487.0000475).
- Gao, Y., Wang, L., Li, D., Gao, Y., 2020. Evaluation of valley topography effects on the seismic stability of earthrockfill dams via a modified valley topography coefficient. *Comput. Geotech.* 128, 103814. <https://doi.org/10.1016/j.compgeo.2020.103814>.
- Goh, Anthony, T.C., 1999. Genetic algorithm search for critical slip surface in multiple-wedge stability analysis. *Can. Geotech. J.* 36(2): 382–391. <https://doi.org/10.1139/t98-110>.
- Gong, J., Zou, D.G., Kong, X.J., Liu, J.M., Chen, K., 2021. The simulation of high compressive stress and extrusion phenomenon for concrete face slabs in CFRDs under strong seismic loads. *Soil. Dyn. Earthq. Eng.* 147 (2), 106792. <https://doi.org/10.1016/j.soildyn.2021.106792>.
- Greco, Venanzio, R., 1996. Efficient Monte Carlo technique for locating critical slip surface. *Geotech. Eng.* 122(7): 517–525. [https://doi.org/10.1061/\(ASCE\)0733-9410\(1996\)122:7\(517\)](https://doi.org/10.1061/(ASCE)0733-9410(1996)122:7(517)).
- Griffiths, D.V., Lane, P.A., 1999. Slope stability analysis by finite elements. *Geotechnique* 49 (3), 387–403. <https://doi.org/10.1680/geot.1999.49.3.387>.
- Guo, P.J., 2010. Effect of density and compressibility on K0 of cohesionless soils. *Acta Geotech.* 5 (4), 225–238. <https://doi.org/10.1007/s11440-010-0125-0>.
- Hossain, M.A., Yin, J.H., 2015. Dilatancy and strength of an unsaturated soil-cement interface in direct shear tests. *Int. J. Geomech.* 15 (5), 04014081. [https://doi.org/10.1061/\(ASCE\)GM.1943-5622.0000428](https://doi.org/10.1061/(ASCE)GM.1943-5622.0000428).
- Hirshikesh, Pramod, A.L.N., Ooi, E.T., Song, C., Natarajan, S., 2021. An adaptive scaled boundary finite element method for contact analysis. *Eur. J. Mech. A-Solid.* 86, 104180. <https://doi.org/10.1016/j.euromechsol.2020.104180>.
- Jaky, J., 1944. The coefficient of earth pressure at rest. *J. Soc. Hungarian Archit. Eng.* 131 (11), 355–358. [https://doi.org/10.1061/\(ASCE\)1090-0241\(2005\)131:11\(1429\)](https://doi.org/10.1061/(ASCE)1090-0241(2005)131:11(1429)).
- Jiang, S.-Y., Du, C.-B., Ooi, E.T., 2019. Modelling strong and weak discontinuities with the scaled boundary finite element method through enrichment. *Eng. Fract. Mech.* 222, 106734. <https://doi.org/10.1016/j.engfractmech.2019.106734>.
- Ke, L.J., Gao, Y.F., Li, D.Y., Zhang, J.W., Ji, J., 2019. Undrained stability analysis of trenches for buried submarine pipelines. *Mar. Georesour. Geotechnol.* 38 (5), 583–594. <https://doi.org/10.1080/1064119X.2019.1604918>.
- Khosravi, M., Khababzian, M., 2012. Presentation of critical failure surface of slopes based on the finite element technique. *Geo-Cong* 536–545. <https://doi.org/10.1061/9780784412121.056>.
- Kim, J.Y., Lee, S.R., 1997. An improved search strategy for the critical slip surface using finite element stress fields. *Comput. Geotech.* 21 (4), 295–313. [https://doi.org/10.1016/S0266-352X\(97\)00027-X](https://doi.org/10.1016/S0266-352X(97)00027-X).
- Kontoe, S., Pelecanos, L., Potts, D., 2013. An important pitfall of pseudo-static finite element analysis[J]. *Comput. Geotech.* 48 (MAR.), 41–50. <https://doi.org/10.1016/j.compgeo.2012.09.003>.
- Kontoe, S., Summersgill, F.C., Potts, D.M., Lee, Y., 2022. On the effectiveness of slope stabilising piles for soils with distinct strain-softening behaviour. *Géotechnique*. 72 (4), 309–321. <https://doi.org/10.1680/jgeot.19.P.386>.
- Krahn, J., 2003. The 2001 R.M. Hardy Lecture: The limits of limit equilibrium analyses. *Can. Geotech. J.* 40 (3), 643–660.
- Li, Y.X., Yang, X.L., 2016. Stability analysis of crack slope considering nonlinearity and water pressure. *KSCE. J. Civ. Eng.* 20 (6), 2289–2296. <https://doi.org/10.1007/s12205-015-0197-3>.
- Li, Y.X., Yang, X.L., 2018. Three-dimensional seismic displacement analysis of rock slopes based on Hoek-Brown failure criterion. *KSCE. J. Civ. Eng.* 22 (11), 4334–4344. <https://doi.org/10.1007/s12205-018-3022-y>.
- Li, X., Liu, J., Gong, W., Xu, Y.I., Bowa, V.M., 2022. A discrete fracture network based modeling scheme for analyzing the stability of highly fractured rock slope. *Comput. Geotech.* 141, 104558. <https://doi.org/10.1016/j.compgeo.2021.104558>.
- Liu, J., Lin, G., 2012. A scaled boundary finite element method applied to electrostatic problems. *Eng. Anal. Boundary. Elem.* 36 (12), 1721–1732. <https://doi.org/10.1016/jenganabound.2012.06.010>.
- Liu, S.Y., Shao, L.T., Li, H.J., 2015a. Slope stability analysis using the limit equilibrium method and two finite element methods. *Comput. Geotech.* 63 (jan.), 291–298. <https://doi.org/10.1016/j.compgeo.2014.10.008>.
- Liu, Y.-r., Wu, Z.-S., Chang, Q., Li, B.o., Yang, Q., 2015b. Stability and reinforcement analysis of rock slope based on elasto-plastic finite element method. *J. Cent. South. Univ.* 22 (7), 2739–2751. <https://doi.org/10.1007/s11771-015-2804-3>.
- Matsui, T., San, K.C., 2008. Finite element slope stability analysis by shear strength reduction technique. *Soils. Found.* 32 (1), 59–70. <https://doi.org/10.3208/sandf1972.32.59>.
- Metaya, S., Chaudhary, N., Sharma, K.K., 2021. Pseudo static stability analysis of rock slope using patton's shear criterion. *Int. J. Geo-Eng.* 12 (1), 1–22. <https://doi.org/10.1186/s40703-020-00137-w>.

- Michalowski, R.L., Drescher, A., 2009. Three-dimensional stability of slopes and excavations. *Geotechnique* 59 (10), 839–850. <https://doi.org/10.1680/geot.8.1336>.
- Nguyen, K.C., Tran, P., Nguyen, H.X., 2019. Multi-material topology optimization for additive manufacturing using polytree-based adaptive polygonal finite elements. *Autom. Constr.* 99, 79–90. <https://doi.org/10.1016/j.autcon.2018.12.005>.
- Nguyen, X.H., Nguyen, H.S., Rabczuk, T., Hackl, K., 2016. A polytree-based adaptive approach to limit analysis of cracked structures. *Comput. Method. Appl. M.* 313, 1006–1039. <https://doi.org/10.1016/j.cma.2016.09.016>.
- Ooi, E.T., Shi, M.G., Song, C.M., Loi, T.F., Yang, Z.M., 2013. Dynamic crack propagation simulation with scaled boundary polygon elements and automatic remeshing technique. *Eng. Fract. Mech.* 106, 1–21. <https://doi.org/10.1016/j.engfracmech.2013.02.002>.
- Ooi, E.T., Song, C., Tin-Loi, F., Yang, Z., 2012. Polygon scaled boundary finite elements for crack propagation modelling. *Int. J. Numer. Methods. Eng.* 91 (3), 319–342. <https://doi.org/10.1002/nme.4284>.
- Ooi, E.T., Song, C.M., Natarajan, S., 2017. A scaled boundary finite element formulation with bubble functions for elasto-static analyses of functionally graded materials. *Comput. Mech.* 60 (6), 1–25. <https://doi.org/10.1007/s00466-017-1443-y>.
- Pang, H.P., Nie, X.P., Sun, Z.B., Hou, C.Q., Dias, D., Wei, B.X., 2020. Upper Bound Analysis of 3D-Reinforced Slope Stability Subjected to Pore-Water Pressure. *Int. J. Geomech.* 20 (4), 06020002. [https://doi.org/10.1061/\(ASCE\)GM.1943-5622.0001636](https://doi.org/10.1061/(ASCE)GM.1943-5622.0001636).
- Pramoda, A.L.N., Ooi, E.T., Song, C.M., Natarajan, S., 2018. Numerical estimation of stress intensity factors in cracked functionally graded piezoelectric materials - A scaled boundary finite element approach. *Compos. Struct.* 206, 301–312. <https://doi.org/10.1016/j.compstruct.2018.08.006>.
- Qu, Y.Q., Zou, D.G., Kong, X.J., Yu, X., Chen, K., 2020. Seismic cracking evolution for anti-seepage face slabs in concrete faced rockfill dams based on cohesive zone model in explicit SBFEM-FEM frame. *Soil. Dyn. Earthq. Eng.* 133(Jun.), 106106.1–106106.14. <https://doi.org/10.1016/j.soildyn.2020.106106>.
- Summersgill, F.C., Kontoe, S., Potts, D.M., 2017. Stabilisation of excavated slopes in strain-softening materials with piles. *Geotechnique* 68 (7), 626–639. <https://doi.org/10.1680/jgeot.17.P.096>.
- Sun, C., Chai, J., Luo, T., Xu, Z., Chen, X., Qin, Y., Ma, B., 2021. Nonlinear shear-strength reduction technique for stability analysis of uniform cohesive slopes with a general nonlinear failure criterion. *Int J Geomech.* 21 (1), 06020033. [https://doi.org/10.1061/\(ASCE\)GM.1943-5622.0001885](https://doi.org/10.1061/(ASCE)GM.1943-5622.0001885).
- Tabarraei, A., Sukumar, N., 2005. Adaptive computations on conforming quadtree meshes. *Finite. Elem. Anal. Des.* 41 (7–8), 686–702. <https://doi.org/10.1016/j.finel.2004.08.002>.
- Tabarraei, A., Sukumar, N., 2007. Adaptive computations using material forces and residual-based error estimators on quadtree meshes. *Comput. Method. Appl. M.* 196 (25–28), 2657–2680. <https://doi.org/10.1016/j.cma.2007.01.016>.
- Tang, H., Yong, R., Ez Eldin, M.A.M., 2017. Stability analysis of stratified rock slopes with spatially variable strength parameters: the case of Qianjiangping landslide. *Bull. Eng. Geol. Environ.* 76 (3), 839–853. <https://doi.org/10.1007/s10064-016-0876-4>.
- Tu, Y.L., Zhong, Z.L., Luo, W.K., Liu, X.R., Wang, S., 2016. A modified shear strength reduction finite element method for soil slope under wetting-drying cycles. *Geomech. Eng.* 11 (6), 739–756. <https://doi.org/10.12989/gae.2016.11.6.739>.
- Wolf, J.P., Schanz, M., 2004. The scaled boundary finite element method. *Comput. Mech.* 33 (4) <https://doi.org/10.1007/s00466-004-0556-2>.
- Wu, S., Xiong, L., Zhang, S., 2018. Strength reduction method for slope stability analysis based on a dual factoring strategy. *Int. J. Geomech.* 18 (10), 04018123. [https://doi.org/10.1061/\(ASCE\)GM.1943-5622.0001249](https://doi.org/10.1061/(ASCE)GM.1943-5622.0001249).
- Xu, J.S., Li, Y.X., Yang, X.L., 2018. Seismic and static 3D stability of two-stage slope considering joined influences of nonlinearity and dilatancy. *KSCE. J. Civ. Eng.* 22 (10), 3827–3836. <https://doi.org/10.1007/s12205-018-0636-z>.
- Yerry, M.A., Shepard, M.S., 1983. A modified quadtree approach to finite element mesh generation. *IEEE Comput. Graph. Appl.* 3 (1), 39–46. <https://doi.org/10.1109/MCG.1983.262997>.
- Yao, W., Hu, B., Ma, C., Zhan, H.B., 2017. Applicability research on the dip slope with Interbeddings of weak and strong rocks using strength reduction method. *Geotech. Geol. Eng.* 35 (3), 1111–1118. <https://doi.org/10.1007/s10706-017-0167-2>.
- Zander, N., Bog, T., Elhaddad, M., Frischmann, F., Kollmannsberger, S., Rank, E., 2016. The multi-level hp-method for three-dimensional problems: Dynamically changing high-order mesh refinement with arbitrary hanging nodes. *Comput. Method. Appl. M.* 310(oct.1), 252–277. <https://doi.org/10.1016/j.cma.2016.07.007>.
- Zhang, Z.H., Liu, Y., Dissanayake, D.D., Saputra, A.A., Song, C.M., 2018. Nonlocal damage modelling by the scaled boundary finite element method. *Eng. Anal. Bound. Elem.* 99 (FEB.), 29–45. <https://doi.org/10.1016/j.enganabound.2018.10.006>.
- Zheng, H., Sun, G.H., Liu, D.F., 2009. A practical procedure for searching critical slip surfaces of slopes based on the strength reduction technique. *Comput. Geotech.* 36 (1–2), 1–5. <https://doi.org/10.1016/j.compgeo.2008.06.002>.
- Zhu, D.Y., 2001. A method for locating critical slip surfaces in slope stability analysis. *Can. Geotech. J.* 38 (2), 328–337. <https://doi.org/10.1139/t00-118>.
- Zienkiewicz, O.C., Humpheson, C., Lewis, R.W., 1975. Associated and non-associated visco-plasticity and plasticity in soil mechanics. *Geotechnique* 25 (4), 671–689. <https://doi.org/10.1680/geot.1975.25.4.671>.
- Zou, D.G., Han, H.C., Liu, J.M., Yang, D.X., Kong, X.J., 2017. Seismic failure analysis for a high concrete face rockfill dam subjected to near-fault pulse-like ground motions. *Soil. Dyn. Earthq. Eng.* 98, 235–243. <https://doi.org/10.1016/j.soildyn.2017.03.031>.
- Zou, D.G., Chen, K., Kong, X.J., Yu, X., 2019. An approach integrating BIM, octree and FEM-SBFEM for highly efficient modeling and seismic damage analysis of building structures. *Eng. Anal. Bound. Elem.* 104, 332–346. <https://doi.org/10.1016/j.enganabound.2019.03.038>.
- Zou, D.G., Kong, X.J., Xu, B., 2005. User manual for geotechnical dynamic nonlinear analysis. Institute of Earthquake Engineering, Dalian University of Technology, Dalian.
- Zou, J.Z., Williams, D.J., Xiong, W.L., 1995. Search for critical slip surfaces based on finite element method. *Can. Geotech. J.* 32 (2), 233–246. <https://doi.org/10.1139/t95-026>.